THE JOURNAL OF PHYSICAL CHEMISTRY C LETTERS

2008, *112,* 8117–8121
Published on Web 05/03/2008

Experimental Verification of the SERS Electromagnetic Model beyond the $|E|^4$ Approximation: Polarization Effects

E. C. Le Ru,*,† J. Grand,‡ N. Félidj,‡ J. Aubard,‡ G. Lévi,‡ A. Hohenau,§ J. R. Krenn,§ E. Blackie,† and P. G. Etchegoin†

The MacDiarmid Institute for Advanced Materials and Nanotechnology, School of Chemical and Physical Sciences, Victoria University of Wellington, P.O. Box 600, Wellington, New Zealand, Laboratoire ITODYS, Université Paris 7, Denis Diderot, CNRS UMR 7086, 1 Rue Guy de la Brosse, F, 75005 Paris, France, and Institute of Physics, Karl Franzens University, Universitätsplatz 5, A-8010 Graz, Austria

Received: March 13, 2008

The failure of the so-called $|E|^4$ approximation of the surface-enhanced Raman scattering (SERS) electromagnetic (EM) enhancement factor is demonstrated experimentally using arrays of highly uniform gold nanoparticles specially designed for this purpose. This is first demonstrated for unpolarized detection, and the interpretation of the results then becomes evident by studying the case of polarized detection. These results provide, at the same time, a clear experimental verification of the generalized EM theory of SERS beyond the $|E|^4$ approximation (*Chem. Phys. Lett.* **2006**, *423*, 63). A nontrivial consequence of these concepts is the almost complete polarization rotation of the SERS signal with respect to the incident polarization. This occurs for a prolate nanoparticle with plasmon resonances peaking on either side of the main spectral range covered by the Raman spectrum of the probe. Finally, we discuss how such experiments can be used to extract some information about the molecular adsorption orientation of the probe.

Introduction

Nanoscale metallic objects, such as metallic nanoparticles (NPs), affect the electromagnetic field in their vicinity dramatically. Under the right conditions, which correspond typically to the excitation of localized surface plasmon (LSP) resonances, large field enhancements can be obtained at (or close to) the surface of metallic nanoparticles. These large field enhancements are exploited in a number of spectroscopic techniques such as surface-enhanced fluorescence (SEF) or surface-enhanced Raman scattering (SERS).[1–3] For SERS, in particular, the Raman signal of an adsorbed molecule can be enhanced by as much as[4] $\sim 10^{10}$. Such an enhancement is obviously very attractive for many applications, such as analytical chemistry (for trace detection), and even single-molecule detection.[5] A full understanding of the SERS effect (discovered more than three decades ago) is still, however, under way. This is primarily due to numerous complications in the interpretations of the experiments, including complex molecular adsorption mechanisms, nonuniformity of the SERS substrate (for colloidal NPs, for example), possible chemical effects such as charge transfer for covalently bound molecules, and so forth. Thirty years down the line from its original discovery, it is still possible (and necessary) to pin down very basic aspects of the SERS enhancement, such as its polarization dependence studied hereafter.

Despite all of the complications, it is now well accepted that the electromagnetic (EM) enhancement is the main contribution to SERS. The mechanisms of this EM enhancement are also described well by classical EM theory.[2,6,7] Within this model, the SERS-EM enhancement factor, F, for a given molecule is usually approximated (in the so-called $|E|^4$ approximation)[9] by

$$F(\mathbf{r}) \approx |\tilde{\mathbf{E}}_{\mathrm{Loc}}(\mathbf{r},\ \omega_{\mathrm{L}})|^2\, |\tilde{\mathbf{E}}_{\mathrm{Loc}}(\mathbf{r},\ \omega_{\mathrm{R}})|^2 \qquad (1)$$

where $\tilde{\mathbf{E}}_{\mathrm{Loc}} = \mathbf{E}_{\mathrm{Loc}}/E_0$ is the local field at the molecule position $\mathbf{r}$ normalized by the incident field amplitude E_0. $|\tilde{\mathbf{E}}_{\mathrm{Loc}}|^2$ is therefore the local field intensity enhancement factor (LFEF),[7,8] taken either at the laser frequency ω_{L} (excitation) or the Raman frequency ω_{R} (emission). The range of validity of this expression (and its generalization) was studied in full detail in ref 7, which will serve as a cornerstone for many of the explanations provided in this Letter.

Experimental verifications of the validity of the SERS EM enhancement are obviously desirable, in particular as a hint of possible additional enhancement mechanisms such as chemical enhancements.[10] The first and arguably most important aspect is the *magnitude* of the enhancement factor (EF). The most recent estimations,[4] in particular using a bianalyte method to identify single-molecule SERS signals,[5] have shown that maximum SERS EFs were typically on the order of $\sim 10^{10}$. This is compatible with the standard EM model of SERS (with eq 1, for example) because EM calculations predict LFEFs up to $|\tilde{\mathbf{E}}_{\mathrm{Loc}}(\omega)|^2 \approx 10^5 - 10^6$. Much more work is nonetheless still needed in this area.

The other feature of eq 1 that can be verified experimentally is the *spectral dependence* of the enhancement, as a function of either ω_{L} or ω_{R}. This spectral response is, in principle, easier to study because it only requires measurements of *relative* SERS EFs (rather than their absolute magnitude). Despite this, it is

* Corresponding author. E-mail address: Eric.LeRu@vuw.ac.nz.
† Victoria University of Wellington.
‡ Laboratoire ITODYS.
§ Karl Franzens University.

10.1021/jp802219c CCC: $40.75

only recently that it has become possible to clearly verify experimentally the validity of this aspect of the EM-enhancement model for SERS, mostly thanks to improvements in the uniformity of nanoparticle-based SERS substrates.[11–13] Even then, only the spectral response of the average SERS EF (rather than the single-molecule EF) was studied. Implicit in these studies was the fact that the ω_L and ω_R dependence could be decoupled in the spatial-averaging of eq. 1; that is

$$\langle F \rangle \approx G\, A(\omega_L)\, A(\omega_R) \qquad (2)$$

where G is a geometrical constant depending on the substrate and $A(\omega)$ characterizes the spectral profile of the average LFEF. Besides, it was further assumed that the extinction profile $Q_e(\omega)$ measured in the far field was a good representation of the spectral profile of the average LFEF; that is, $A(\omega) \propto Q_e(\omega)$. Both properties indeed have the same physical origin: coupling to the LSP resonances. Although intuitive, these assumptions are far from obvious, but they can be shown to be valid at least for simple structures like spherical nanoparticles.[14] Within these assumptions, it is possible to verify the validity of eq 2 by comparing the measured average SERS EF with the extinction profile of the substrate. Using a series of SERS substrates with varying LSP resonance wavelengths (i.e., changing $A(\omega)$), this was demonstrated on gold NP arrays fabricated by e-beam lithography[11] and on silver nanotriangles fabricated by nanosphere lithography.[13] These results were further confirmed using a more direct approach of varying the excitation frequency (ω_L) directly on a given SERS substrate (so-called wavelength-scanned surface-enhanced Raman excitation spectroscopy).[15,20] More recently, the ω_R dependence was further verified by studying directly the SERS EF of several SERS peaks (with different ω_R) of the same analyte.[16,17] It is also interesting to note in this context that this spectral dependence of the LFEF also affects the fluorescence spectrum of fluorescing molecules drastically, thereby providing an additional probe of the underlying LFEF.[18] Finally, other recent studies have also demonstrated the validity of the SERS EM model in the $|E|^4$ approximation as a function of distance from the surface[19,20] and in gap hot-spots between two metallic objects.[21,22]

In this Letter, we go one step further by highlighting a striking example of the failure of the $|E|^4$ approximation and providing experimental verification of the SERS-EM model beyond this approximation. To put this into context, we first focus on the results of Figure 1, where the $|E|^4$ approximation is valid. Figure 1c shows the SERS spectrum of Rhodamine 6G (RH6G) adsorbed on two different arrays of gold oblate NPs (i.e., with circular cross-section). The intensity of each SERS peak is obtained from a fit and normalized to the corresponding non-SERS intensity to yield a relative average EF, $\langle F_R(\omega_R)\rangle$, as detailed in the Supporting Information. Following eq 2 and the previous discussion, $\langle F_R(\omega_R)\rangle$ should have the same spectral profile (ω_R dependence) as the extinction spectrum $Q_e(\omega_R)$. This is indeed the case, as shown in Figure 1d, and simply confirms the results of previous studies.[11–13,15,17] We note here that the fluorescence background in the SERS spectra of Figure 1c also reflects the profile $Q_e(\omega_R)$ directly (convoluted with the fluorescence profile of bare RH6G).[18] Both approaches, relative EF of the SERS peaks and fluorescence background, can therefore be used to reveal the underlying LFEF spectral profile.

These results are now compared with the example of Figure 2 where prolate NPs (i.e., with elliptic, rather than circular, cross sections), are used instead. Such NPs exhibit two LSP resonances, each associated with one of the two principal axes (in the $X-Y$ plane).[2,23] The extinction spectra, $Q_e^X(\omega)$ for X polarization (along the long axis) and $Q_e^Y(\omega)$ for Y polarization (along the short axis) are shown in Figure 2b. It clearly shows

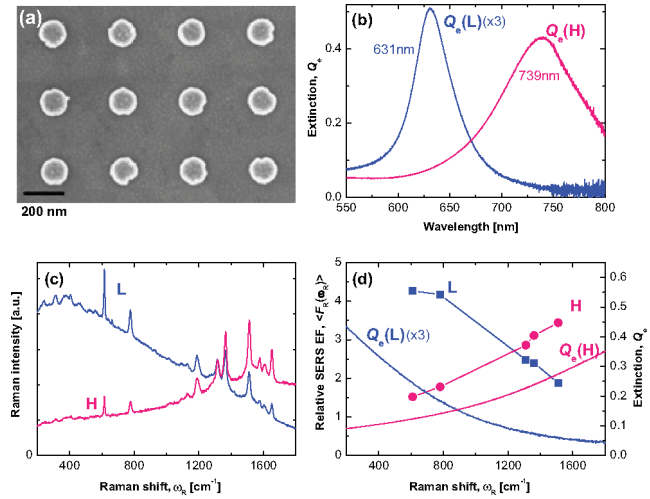

Figure 1. (a) Representative SEM image of an array of gold oblate NPs (i.e., the circular section of which is oriented normally to the ITO substrate surface). (b) Extinction spectrum for two arrays of oblate particles of height ~50 nm and diameter 100 nm (L) and 160 nm (H), respectively. (c) Corresponding SERS spectra at 633-nm excitation (with the ITO background subtracted) after dipping arrays L and H in a 10^{-5} M Rhodamine 6G solution. (d) Comparison between the relative EFs of the SERS peaks (symbols) and the extinction profile for each array (lines).

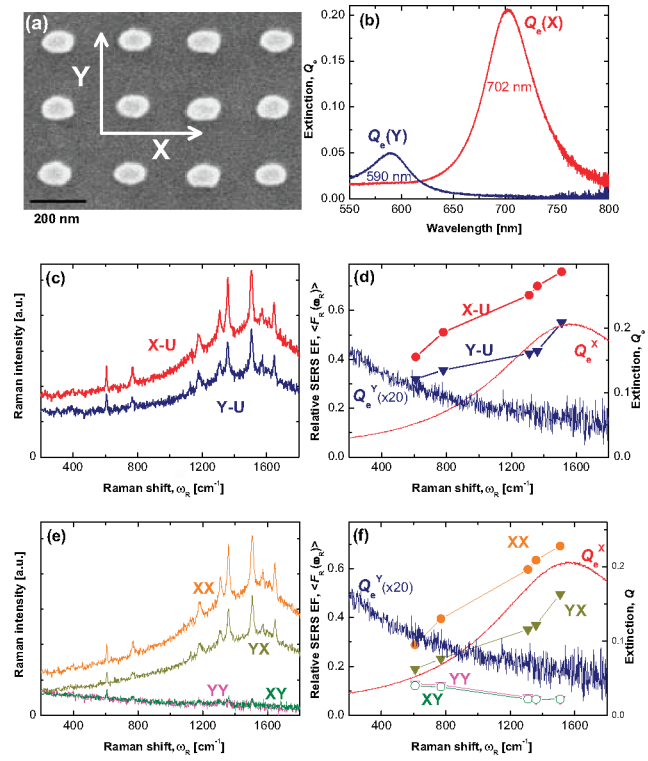

Figure 2. (a) Representative SEM image of gold prolate NPs. Height is ~50 nm and dimensions in the plane are 140 nm (X) by 90 nm (Y) (b) Extinction spectrum for X- and Y-polarized excitation. (c) Corresponding SERS spectra at 633-nm excitation (with unpolarized detection) after dipping the array in a 10^{-5} M RH6G solution. (d) Comparison between the relative average EFs $\langle F_R(\omega_R)\rangle$ (symbols) of the SERS peaks in (c) and the extinction profile $Q_e(\omega_R)$ (lines) in part b for each excitation polarization. (e) SERS spectra for the four excitation-detection ($ED = XX, XY, YX, YY$) polarization configurations. (f) Comparison of the relative SERS EFs in part e with the extinction profiles of part b.

TABLE 1: Summary of the Results Obtained from Fits to the SERS Peaks (Characterized by Their Raman Shift ω_R) after Dipping the NP Array of Figure 2 in a Solution of Rhodamine 6G (RH6G), Crystal Violet (CV), or BTZ2[a]

rhodamine 6G						crystal violet						BTZ2					
ω_R	ρ^X	ρ^Y	μ^X	μ^Y	$\rho^X\rho^Y$	ω_R	ρ^X	ρ^Y	μ^X	μ^Y	$\rho^X\rho^Y$	ω_R	ρ^X	ρ^Y	μ^X	μ^Y	$\rho^X\rho^Y$
						(cm−1)	I^{XY}/I^{XX}	I^{YX}/I^{YY}	I^{YX}/I^{XX}	I^{XY}/I^{YY}						
612	0.42	1.46	0.66	0.93	0.61	210	0.23	1.30	0.29	1.04	0.30	480	0.23	0.98	0.40	0.55	0.22
774	0.29	1.86	0.59	0.93	0.54	441	0.19	1.49	0.28	1.01	0.28	1108	0.08	2.29	0.38	0.47	0.18
1311	0.11	4.77	0.59	0.90	0.53	917	0.07	4.33	0.27	1.19	0.32	1400	0.06	4.05	0.40	0.58	0.23
1364	0.10	5.66	0.58	1.00	0.58	1177	0.05	5.36	0.29	0.93	0.27	1617	0.04	4.17	0.42	0.41	0.17
1511	0.09	7.56	0.72	1.00	0.72	1621	0.03	8.71	0.31	0.89	0.27						

[a] The ratios ρ^X, ρ^Y, μ^X, and μ^Y are defined as ratios of SERS peak intensities for two of the four polarization configurations: *XX*, *XY*, *YX*, and *YY*.

that, with an appropriate choice of the polarization of the excitation, only one resonance or the other can be excited. The corresponding SERS spectra with *E*-polarized excitation ($E = X, Y$) are shown in Figure 2c. One could expect, by analogy with the previous results, that $\langle F_R^E(\omega_R)\rangle$ should follow $Q_e^E(\omega_R)$. As shown in Figure 2d, this is indeed the case for $E = X$, but certainly not for *Y*-polarized excitation. In fact, despite the fact that the SERS signal is excited with *Y* polarization, the EF spectral profile seems to follow $Q_e^X(\omega_R)$; that is, the LFEF of the other polarization. This can in fact be understood in simple terms: from the point of view of the excitation of the Raman dipole, only the normalized local field $\tilde{\mathbf{E}}_{Loc}^Y(\omega_L)$ for *Y* polarization matters. However, the radiation pattern and intensity of this Raman dipole are in general affected by both LSP resonances (*X* and *Y*). Because the *X* resonance, associated with the long axis, is stronger in this example in the region of Raman emission, it naturally imposes its spectral dependence onto the SERS EF. The common $|E|^4$ approximation no longer applies in its standard form (eqs 1 or 2) in this case.

In order to place this qualitative argument on a stronger footing, we will specialize the discussion to our experimental setup. We consider a SERS experiment in the back-scattering configuration, where the incident beam is incoming along *Z* (with *X* or *Y* polarization) and detected with the same optics along *Z* . The SERS signal can be analyzed into two polarizations (*X* and *Y*). The exciting polarization is denoted *E* and the detection polarization, *D* . We then have four possible excitation/detection polarization configurations[24] *ED*: *XX*, *XY*, *YX*, and *YY*. The theoretical description of the EM SERS EF for these four configurations, and in particular the rigorous use of the optical reciprocity theorem, have been described in ref 7, which we adapt here to our problem. We denote $\tilde{\mathbf{E}}_{Loc}^E(r, \omega)$ ($E = X, Y$) the normalized local field for plane wave excitation with *E* polarization at frequency ω. This can, in principle, be predicted from the solution of Maxwell's equations for two distinct EM problems (one for each polarization). Let us now consider a molecule at a position $\mathbf{r}$ (typically adsorbed on the surface of the NP) and a Raman mode with a Raman polarizability tensor $\hat{\alpha}$. The single-molecule SERS EF for a SERS experiment in the general configuration *ED* is then obtained from a generalization of eq 1 as

$$F^{ED}(\mathbf{r}) = |\tilde{\mathbf{E}}_{Loc}^D(\mathbf{r}, \omega_R) \cdot \hat{\alpha}_N \cdot \tilde{\mathbf{E}}_{Loc}^E(\mathbf{r}, \omega_L)|^2 \qquad (3)$$

where $\hat{\alpha}_N$ is the normalized Raman polarizability tensor (proportional to the Raman polarizability tensor) as defined rigorously in ref 4. Note that an equivalent expression for unpolarized detection (common in SERS experiments) can be obtained simply by summing the result for configurations *EX* and *EY* . It is then clear that even for a fixed polarized excitation *E* both resonances (*X* and *Y*) affect the SERS signal for unpolarized detection.

In many SERS experiments, including those reported here, the signal originates from an ensemble of molecules covering uniformly the surface. Because the local fields are typically nonuniform (in both magnitude and orientation) on the surface, the measured enhancement is then the position-averaged analog of eq 3, $\langle F^{ED}\rangle$. As for the $|E|^4$ approximation, the various factors in this average cannot in the most general case be deconvolved, but let us assume as before (and for the same reasons) that it is possible to write the average EF as the analog of eq 2:

$$\langle F^{ED}\rangle \approx J_{ED}\, A^E(\omega_L)\, A^D(\omega_R) \qquad (4)$$

J_{ED} is a geometrical factor like *G* in eq 2, depending in addition on the symmetry of the Raman tensor (characterized by $\hat{\alpha}_N$) and the experiment configuration (*ED*). $A^E(\omega)$ characterizes the average LFEF for *E* polarized excitation ($E = X, Y$). As before, its spectral profile can be assumed to follow that of the extinction spectrum for the same polarized excitation: $A^E(\omega) \approx Q_e^E(\omega)$. This expression suggests that the separate effects of the LFEF of each resonance (*X* and *Y*) on the SERS signal can be studied by measuring the SERS spectrum in the four configurations *XX*, *YX*, *XY*, and *YY*. This is shown explicitly in Figure 2e−f, which we now discuss in relation to eq 4.

First, the spectral profile in emission (i.e., the ω_R dependence) should be, according to eq 4, determined by $A^D(\omega_R) \approx Q_e^D(\omega_R)$, that is, by the LSP resonance profile for *D*-polarized excitation and not by that for *E*-polarized excitation (as the conventional $|E|^4$ approximation would suggest because the experiment is indeed performed with *E*-polarized excitation). This is clear in Figure 2e−f: configurations *XX* and *YX* follow the spectral profile of Q_e^X, whereas *XY* and *YY* follow that of Q_e^Y. The results in Figure 2e−f therefore provide a *clear experimental demonstration of the SERS EM model beyond the* $|E|^4$ *approximation*.[7] Note that the distinction between the four configurations in fact also explains the result of Figure 2c and d (unpolarized detection) because *YU* is simply the sum of *YX* (strong) and *YY* (weak) and is therefore similar to *YX*; therefore, it follows Q_e^X despite the *Y*-polarized excitation.

Second, the fits of the SERS peak intensities I^{ED} for the four configurations enable us to calculate system-independent ratios:

$$\rho^X = \frac{I^{XY}}{I^{XX}},\ \rho^Y = \frac{I^{YX}}{I^{YY}},\ \mu^X = \frac{I^{YX}}{I^{XX}},\ \mu^Y = \frac{I^{XY}}{I^{YY}} \qquad (5)$$

ρ^X and ρ^Y correspond to the *depolarization ratios* of the SERS peaks for *X* and *Y* excitation, respectively. μ^X and μ^Y are new concepts and can be thought of as "reverse depolarization ratios". The measured values of these ratios are summarized in Table 1 for the experiments of Figure 2 with RH6G, and for similar experiments performed on the same NP array but with different analytes: crystal violet (CV) and BTZ2 (dye no. 2 of ref 25). Particularly striking in this table are the

values of the depolarization ratios ρ^Y for *Y*-polarized excitation. Values larger than 1 are obtained for most peaks and almost up to $\rho^Y \approx 8$ is measured for the highest-energy Raman peaks. This is in fact a direct consequence of eq 4 when the LSP resonances for *Y*- and *X*-polarized excitation peak on either side of the Raman spectral range (see Figure 2b). Nevertheless, it is worth stressing that ρ is always between 0 and $^3/_4$ for normal molecular Raman scattering in liquids.[26] What we observe here is that the polarization of the SERS signal is almost entirely rotated by 90° compared to excitation. This highlights again the necessity to generalize the $|E|^4$ approximation (eqs 1 and 2) to the expressions given in eqs. 3 and 4. It also provides, by the same token, a striking example of *polarization rotation induced by plasmon resonances in a Raman process*.

We conclude this Letter by discussing qualitatively how the results of Table 1 may be further exploited. The ratios ρ^E and μ^D can be expressed explicitly using eq 4, for example

$$\rho^X = \frac{J_{XY}}{J_{XX}} \frac{A^Y(\omega_R)}{A^X(\omega_R)}, \quad \mu^X = \frac{J_{YX}}{J_{XX}} \frac{A^Y(\omega_L)}{A^X(\omega_L)} \tag{6}$$

Another interesting quantity is the product

$$\rho^X \rho^Y = \mu^X \mu^Y = \frac{J_{XY} J_{YX}}{J_{XX} J_{YY}} \tag{7}$$

The main difficulty in comparing these expressions to the experimental results lies in the geometrical factors J_{ED}. They depend on the substrate geometry and the surface selection rules[8,27] (Raman tensor and adsorption orientation of the probe), and a theoretical model is required to make a quantitative connection. In the case at hand here, one can solve the EM problem analytically by considering gold ellipsoids in the electrostatics approximation.[23] This enables us to justify the validity of eq 4 and provides a connection between the factors J_{ED} and the orientation/Raman tensors of the probe. Such a detailed analysis is outside the scope of this Letter and will be reported elsewhere. We will instead provide a more general qualitative discussion of the experimental results of Table 1. We focus first on the product in eq 7, which depends only on the geometrical factors J_{ED}. From Table 1, it appears that for a given molecule $\rho^X\rho^Y$ is approximately independent of the Raman peak. This suggests that the Raman peaks under consideration have, for a given molecule, a similar Raman tensor symmetry. This is in fact expected for molecules under resonant or preresonant Raman conditions.[4] This product, however, does seem to differ for different molecules: ~0.65 for RH6G, ~0.28 for CV, and ~0.2 for BTZ2. This discrepancy must be a result of a different molecular orientation (and possibly Raman tensor) across the three probes, that is, of SERS surface selection rules.[8,27] Regarding the depolarization ratios ρ^X (and ρ^Y), it is clear from eq 6 that the peak-to-peak variation is dominated by the ω_R dependence of the ratio $A^Y(\omega_R)/A^X(\omega_R)$, as confirmed by the experimental results of Table 1. The "reverse depolarization ratios" μ^X and μ^Y are, however, not affected by this dependence and should therefore, up to the surface selection rules effect (the factors J_{ED}), be independent of the Raman shift ω_R for a given molecule. This is indeed what we observe experimentally in Table 1. Moreover, the discrepancy in the values of μ^D across molecules can be attributed to the same reasons as those discussed for the product $\rho^X\rho^Y$. There is also the additional possibility of a small change in the LSP resonances, and therefore in the ratio $A^Y(\omega_L)/A^X(\omega_L)$, as a result of different adsorbates on the NPs[28] (which we do observe experimentally in the extinction spectra). Regardless of the difficulties in the details (which will be studied in full elsewhere), the above arguments illustrate how eq 4 can be combined with some additional modeling and careful polarization-dependent SERS experiments to probe the surface adsorption properties of the analyte (despite the ensemble averaging); a very difficult property to measure by all standards.

In closing, using arrays of highly uniform prolate (asymmetric) gold nanoparticles, we have provided a clear experimental verification of the SERS electromagnetic enhancement factor beyond the $|E|^4$ approximation. A spectacular consequence of these concepts is the almost complete polarization rotation of the SERS signal with respect to the incident polarization for a prolate particle with appropriate LSP resonances (with respect to the laser wavelength). Furthermore, we propose that this approach may be used in the future as a probe of the analyte orientation of the surface.

Acknowledgment. This work was supported by the Dumont d'Urville France/NZ exchange programme. E.C.L.R. and P.G.E. acknowledge partial support from a Marsden Grant of the Royal Society of New Zealand (RSNZ).

Supporting Information Available: Non-SERS properties of Rhodamine 6G for the calculation of relative average SERS EFs. This material is available free of charge via the Internet at http://pubs.acs.org.

References and Notes

(1) Metiu, H. *Prog. Surf. Sci.* **1984**, *17*, 153. and references therein.
(2) Moskovits, M. *Rev. Mod. Phys.* **1985**, *57*, 783.
(3) Aroca, R. *Surface Enhanced Vibrational Spectroscopy*; Wiley: Chichester, 2006.
(4) Le Ru, E. C.; Blackie, E.; Meyer, M.; Etchegoin, P. G. *J. Phys. Chem. C* **2007**, *111*, 13794.
(5) Le Ru, E. C.; Meyer, M.; Etchegoin, P. G *J. Phys. Chem. B* **2006**, *110*, 1944.
(6) Schatz, G. C.; Young, M. A.; Van Duyne, R. P. *Top. Appl. Phys.* **2006**, *103*, 19.
(7) Le Ru, E. C.; Etchegoin, P. G. *Chem. Phys. Lett.* **2006**, *423*, 63.
(8) Le Ru, E. C.; Meyer, M.; Blackie, E.; Etchegoin, P. G. *J. Raman Spectrosc.* **2008**, in press.
(9) Note that some authors use the term $|E|^4$ approximation only when the additional approximation of a negligible Raman shift (i.e., $\omega_R \approx \omega_L$) is made.
(10) Otto, A. *J. Raman Spectrosc.* **1991**, *22*, 743.
(11) Félidj, N.; Aubard, J.; Lévi, G.; Krenn, J. R.; Salerno, M.; Schider, G.; Lamprecht, B.; Leitner, A.; Aussenegg, F. R. *Phys. Rev. B* **2002**, *65*, 75419.
(12) Félidj, N.; Aubard, J.; Lévi, G.; Krenn, J.R.; Hohenau, A.; Schider, G.; Leitner, A.; Aussenegg, F. R *Appl. Phys. Lett.* **2003**, *82*, 3095.
(13) Haynes, C. L.; Van Duyne, R. P. *J. Phys. Chem. B* **2003**, *107*, 7426.
(14) Messinger, B. J.; von Raben, K. U.; Chang, R. K.; Barber, P. W. *Phys. Rev. B* **1981**, *24*, 649.
(15) McFarland, A. D.; Young, M. A.; Dieringer, J. A.; Van Duyne, R. P. *J. Phys. Chem. B* **2005**, *109*, 11279.
(16) Le Ru, E. C.; Dalley, M.; Etchegoin, P. G. *Curr. Appl. Phys.* **2006**, *6*, 411.
(17) Le Ru, E. C.; Etchegoin, P. G.; Grand, J.; Félidj, N.; Aubard, J.; Lévi, G.; Hohenau, A.; Krenn, J. R. *Curr. Appl. Phys.* **2008**, *8*, 467.
(18) Le Ru, E. C.; Etchegoin, P. G.; Grand, J.; Félidj, N.; Aubard, J.; Lévi, G. *J. Phys. Chem. C* **2007**, *111*, 16076.
(19) Lal, S.; Grady, N. K.; Goodrich, G. P.; Halas, N. J. *Nano Lett.* **2006**, *6*, 2338.
(20) Dieringer, J. A.; McFarland, A. D.; Shah, N. C.; Stuart, D. A.; Whitney, A. V.; Yonzon, C. R.; Young, M. A.; Zhang, X.; Van Duyne, R. P. *Faraday Discuss.* **2006**, *132*, 9.
(21) Svedberg, F.; Li, Z.; Xu, H.; Kall, M. *Nano Lett.* **2006**, *6*, 2639.
(22) Lee, S. J.; Guan, Z.; Xu, H.; Moskovits, M. *J. Phys. Chem. C* **2007**, *111*, 17985.

(23) Wokaun, A. *Solid State Phys.* **1984**, *38*, 223.
(24) Note that, experimentally, the polarization analyzer for detection is kept unchanged to eliminate any effect of the polarization response of our system. The four configurations are obtained by rotating the laser polarization and/or the NP arrays.
(25) Graham, D.; McLaughlin, C.; McAnally, G.; Jones, J. C.; White, P. C.; Smith, W. E. *Chem. Commun.* **1998**, 1187.
(26) Long, D. A. *The Raman Effect, A Unified Treatment of the Theory of Raman Scattering by Molecules*; Wiley: Chichester, 2002.
(27) Moskovits, M. *J. Chem. Phys.* **1982**, *77*, 4408.
(28) Zhao, J.; Jensen, L.; Sung, J.; Zou, S.; Schatz, G. C.; Van Duyne, R. P. *J. Am. Chem. Soc.* **2007**, *129*, 7647.

JP802219C

Supporting information for "Experimental verification of the SERS electromagnetic model beyond the $|E|^4$-approximation: polarization effects"

S.I. RHODAMINE 6G IN NON-SERS CONDITIONS

The Raman/Fluorescence spectrum, excited at 633 nm, of a solution of 10^{-4} M Rhodamine 6G is shown in Fig. S1. Note that the true residual fluorescence background of RH6G can only be measured accurately if the instrumental and water background is measured under the same conditions and removed (see inset of Fig. S1). The Raman peaks are then clearly seen on top of the residual fluorescence. A fit to the Raman peaks characterized by their Raman frequency ω_R then yields their reference integrated intensity $I_0(\omega_R)$. Similar fits to the same peaks are carried out for all SERS experiments on the nano-particle arrays to yield the SERS intensity $I(\omega_R)$. The relative average SERS EF of each peak is then defined simply as:

$$\langle F_R(\omega_R)\rangle = \frac{I(\omega_R)}{I_0(\omega_R)} \tag{S1}$$

The five peaks with Raman shifts of 612, 774, 1311, 1364, and 1511 cm^{-1} are used to characterize the spectral profile of $\langle F_R(\omega_R)\rangle$.

Examples of relative SERS EFs are given in Figs. 1(d), 2(d) and 2(f) of the main text. $\langle F_R(\omega_R)\rangle$ is in arbitrary units but the same (arbitrary) units are used throughout this study.

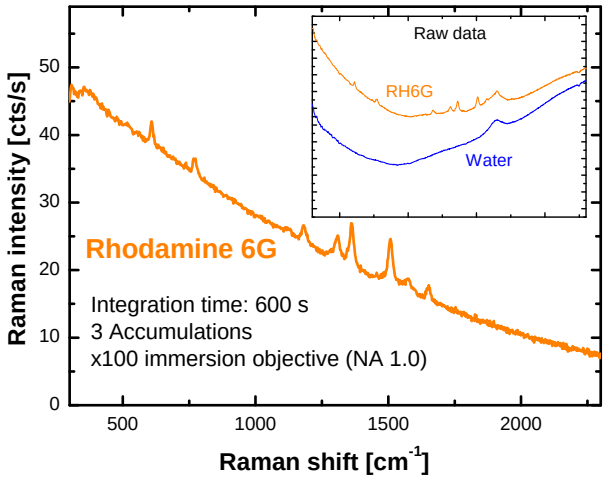

FIG. S1: Raman (non-SERS) spectrum of a 10^{-4} M Rhodamine 6G solution (in water). The raw spectrum is shown in the inset, along with an identical measurement on pure water. The corrected spectrum is then simply obtained by subtraction. Several Raman peaks are clearly resolved above a residual fluorescence background.